Eur. Phys. J. A **10**, 73–84 (2001)

THE EUROPEAN PHYSICAL JOURNAL A

Decay of proton-rich nuclei between ^{39}Ti and ^{49}Ni

J. Giovinazzo[1,a], B. Blank[1], C. Borcea[2], M. Chartier[1], S. Czajkowski[1], G. de France[3], R. Grzywacz[4,b], Z. Janas[4], M. Lewitowicz[3], F. de Oliveira Santos[3], M. Pfützner[4], M.S. Pravikoff[1], and J.C. Thomas[1]

[1] Centre d'Etudes Nucléaires de Bordeaux-Gradignan, Le Haut-Vigneau, B.P. 120, F-33175 Gradignan Cedex, France
[2] Institute of Atomic Physics, P.O. Box MG6, Bucharest-Margurele, Romania
[3] Grand Accélérateur National d'Ions Lourds, B.P. 5027, F-14076 Caen Cedex, France
[4] Institute of Experimental Physics, University of Warsaw, PL-00-681 Warsaw, Hoza 69, Poland

Received: 26 July 2000 / Revised version: 22 November 2000
Communicated by C. Signorini

Abstract. Decay studies of very neutron-deficient nuclei ranging from ^{39}Ti to ^{49}Ni have been performed during a projectile fragmentation experiment at the GANIL/LISE3 separator. For all nuclei studied in this work, ^{39,40}Ti, ^{42,43}Cr, ^{46}Mn, ^{45,46,47}Fe and ^{49}Ni, half-lives and decay spectra have been measured. In a few cases, γ coincidence measurements helped to successfully identify the initial and final states of transitions. In these cases, partial decay scheme are proposed. For the most exotic isotopes, ^{39}Ti, ^{42}Cr, ^{45}Fe and ^{49}Ni, which are candidates for two-proton radioactivity from the ground state, no clear evidence of this process is seen in our spectra and we conclude rather on a delayed particle decay.

PACS. 27.40.+z $39 \leq A \leq 58$ – 21.10.Dr Binding energies and masses – 23.50.+z Decay by proton emission – 25.70.Mn Projectile and target fragmentation

1 Introduction

Up to the $A = 50$ mass region, the proton drip-line has been reached experimentally. The observation of nuclei very close to this limit of existence was possible due to recent developments of projectile fragmentation facilities. Indeed, in the mass region we are interested in here, a recent experiment at the GSI/FRS facility allowed for the observation of ^{42}Cr ($T_z = -3$) as well as of ^{45}Fe and ^{49}Ni ($T_z = -7/2$) [1]. During an experiment at the GANIL/LISE3 separator, the existence of these isotopes has been confirmed with increased statistics and ^{48}Ni has been observed for the first time [2].

When going close to the proton drip-line, the emission of two protons from a nuclear state becomes possible. This decay mode is mainly sequential if the emission of one proton can occur to an intermediate state. This process has first been observed in the β2p decay of ^{22}Al [3]. Other two-proton emissions from an excited state have been studied, mainly in the region from $A = 20$ to 40 [4–8], but no evidence of a non-sequential decay could be pointed out.

If there is no accessible intermediate state, the sequential emission is forbidden, and the emission of the two protons is simultaneous. This situation is mainly expected to occur from nuclear ground states. Then two cases are possible. Firstly, the decay may proceed via a three-body disintegration as observed for ^{12}O [9] or ^{6}Be [10]. Secondly, the nuclear state may decay via ^{2}He emission and a strong angular and energy correlation between the two resulting protons may be expected. Up to now, this second process has never been observed experimentally.

In the $A \simeq 50$ mass region, a specific interest arises for decay studies since several nuclei in this region are candidates for this correlated emission of two protons from the ground state: ^{39}Ti, ^{42}Cr, ^{45}Fe, ^{48,49}Ni [11–13]. In addition, full shell-model calculations in the fp-shell are now possible [14] and may allow for a valuable comparison with experimental results to improve our understanding of nuclear structure in this region and to deduce effective interactions.

In the present experiment, we have studied the decay of the isotopes ^{39,40}Ti, ^{42,43}Cr, ^{46}Mn, ^{45,46,47}Fe and ^{49}Ni, for which only few experimental information was available. The nucleus studied in most detail prior to our experiment is ^{40}Ti [15,16] which will be used as a reference for calibration. For ^{39}Ti, the half-life and the main decay branches, including the β2p decay, have been observed previously [17,18]. Some information, like rough lifetime estimates and a few delayed proton lines, is also available for ^{43}Cr, ^{46}Mn and ^{46,47}Fe [19]. For the most exotic isotopes, ^{42}Cr, ^{45}Fe and ^{49}Ni, only their existence was reported [1].

In the present work, we take advantage of the delayed proton emission to determine a precise half-life of the iso-

[a] e-mail: giovinaz@cenbg.in2p3.fr
[b] *Present address*: Department of Physics and Astronomy, University of Tennessee, Knoxville, TN 37996-1200, USA

topes of interest. Many transitions by proton emission are observed, but only few of them could be placed in a partial decay scheme. For the most abundantly produced isotopes, some γ lines have been registered in coincidence with protons yielding valuable information on the decay schemes. Clearly identified transitions also allowed us to determine the position of the isobaric analog state (IAS) in some daughter nuclei and thus, by means of the isobaric multiplet mass equation (IMME), to get an estimate for the mass excess of the exotic emitter nuclei.

2 Experimental procedure

Neutron-deficient nuclei have been produced in the fragmentation reaction of a $^{58}Ni^{26+}$ primary beam at 74.5 MeV/nucleon from the GANIL facility. The 230.6 mg/cm^2 thick natural nickel production target and the 2.7 mg/cm^2 carbon stripper were located between the solenoids of the SISSI device [20]. The most exotic isotopes have been selected with the Alpha spectrometer and the LISE3 [21] separator, including a shaped degrader (10.4 mg/cm^2 of beryllium) at the intermediate focal plane and a Wien filter at the end of the LISE3 beam line.

The selected isotopes have been implanted in a silicon telescope. The telescope consisted (see fig. 1) in two silicon detectors ($\Delta E1$ and $\Delta E2$) for energy-loss measurements (300 μm each, 600 and 30×30 mm^2), the second one being position sensitive. The ions were implanted in a third silicon diode, $E3$ (600 mm^2 surface and 300 μm thickness). Two additional silicon detectors ($E4$ with 450 mm^2 surface and 700 μm thickness and $E5$ with 600 mm^2 surface and 6 mm thickness) were used to veto particles which were not stopped in the previous diodes. The use of two veto detectors is usually not required. However, it was initially planned to implant the ions of interest in the fourth detector and to use only the last one as a veto. This procedure had to be changed in order to correctly identify ^{48}Ni with a maximum of parameters (see [2]). Therefore, no trigger was properly set up for radioactivity events in the $E3$-detector. Radioactivity events were triggered only by β particles in the second and fourth detector leading to an efficiency of $(38 \pm 3)\%$ (see below). For each of the detectors $E2$, $E3$, and $E4$, two electronic chains with different amplification gains were used for implantation and radioactivity events.

The isotope identification was achieved by energy-loss and residual-energy measurements in the telescope and by time-of-flight measurements. Details of the identification procedure are given in ref. [2].

This set-up was surrounded by three germanium detectors, a single cristal and two four-cristal clovers. The total efficiency was measured to be 1.12% at 1.17 MeV. The γ detectors were only used for coincidences and did not appear in the trigger logic of the acquisition.

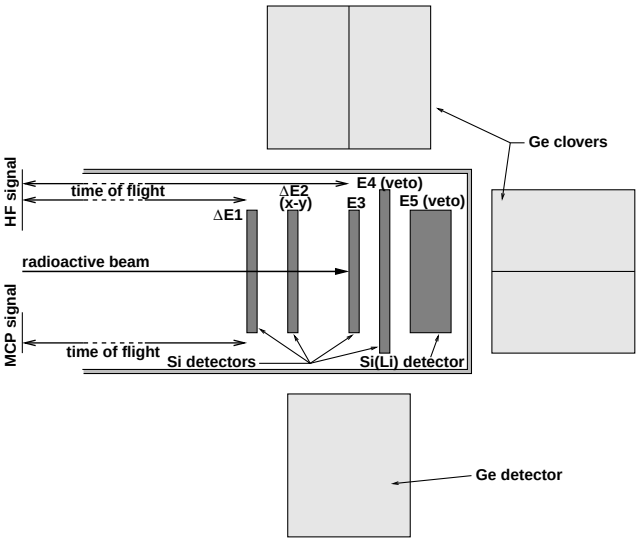

Fig. 1. Detection set-up: Ions are implanted in the $E3$-detector. The identification of isotopes is performed with the $\Delta E1$ and $\Delta E2$ energy loss information, several time-of-flight measurements, the total energy and position measurements. For details, see ref. [2].

3 Data analysis

As described in the paper on the ^{48}Ni observation [2], the identification of isotopes is performed on the basis of a total-energy *vs.* energy-loss matrix. For this purpose, the low-gain electronic chains for the $E1$, $E2$, and $E3$ detectors were calibrated by means of simulations with the LISE [22] program. Additional conditions were imposed on the position in the $E2$ detector, the different times of flight, and the signals in the veto detector.

A clock with a 100 μs step was used for time correlations between radioactivity and implantation events. In the analysis, each radioactivity event following an implantation is taken into account as long as no further implantation did occur. Although the implantation rate was about 10 ions per second in the $E3$-detector, most of those isotopes lie much closer to stability (with long half-lifes) and do not emit delayed protons. Consequently, the correlation procedure is stopped only after the implantation of a relatively exotic nucleus defined by a large window around nuclei of interest in the $\Delta E - E$ matrix. Simulations have been performed using the experimental time distributions i) for all nuclei and ii) for the most exotic ones only. They clearly demonstrated that the determination of half-lives lower than 100 ms do not require any correction for the cut introduced by following implantations. A correction would be needed, on the contrary, if this cut were performed by any implantation instead of the most exotic ones only.

In order to reduce the background from the decay of long-lived isotopes accumulated in the implantation detector, we will analyse proton energy distributions with a condition on events above 1 MeV. This cut removes almost all β events that represent the main background, while most of the proton strength is distributed at higher energies.

The fits for half-life determination are performed with the maximum-likelyhood method from the PAW/MINUIT software [23]. When the proton emission feeds a nucleus that does not decay by proton emission, *i.e.* there is no contamination from protons of the daughter decay in the energy spectrum, an exponential function with a constant background is used for the fit. This concerns the decays of ^{40,39}Ti, ^{43}Cr, ^{46}Mn and ^{47}Fe. For the other isotopes, ^{42}Cr, ^{46,45}Fe and ^{49}Ni, the delayed proton emission from the daughter nucleus is included in the fitting procedure. The error bars include statistical and systematic errors. The systematic errors are mainly due to the time window used for the fitting procedure and to the proton energy cut. These systematic errors were determined by changing both the time and energy cuts. They vary between 20% and 50% of the total error.

The proton energy calibration is obtained from the peaks at 1702, 2162 and 3733 keV in the decay of ^{40}Ti [16, 15]. Due to the summing of proton and β-particles energies, the proton peaks have to be fitted with a Gaussian and an exponential tail plus an exponential background due to lower-energy proton groups. ^{40}Ti together with ^{43}Cr is also used to estimate the trigger efficiency for radioactivity events after implantation. This efficiency is estimated from the fit of the decay time distribution: The number of counts for events with an energy above 1 MeV is compared to the number of implantations. With the additional information that, for ^{40}Ti, the total proton branching ratio above 1 MeV is $(97 \pm 2)\%$ [16], we deduce a detection efficiency $\epsilon_P = (39 \pm 2)\%$ from the decay of this nucleus. Due to the high Q_{EC} value (~ 16 MeV) and the low proton separation energy of only about 200 keV in ^{43}V, we assume that $(95 \pm 5)\%$ of the decay of ^{43}Cr proceeds by delayed particle emission. The resulting detection efficiency for radioactive events is then $\epsilon_P = (37 \pm 2)\%$. In the following, we will use a mean value of $\epsilon_P = (38 \pm 3)\%$ for the trigger efficiency for radioactivity events.

4 Results

4.1 The decay of ^{40}Ti

As mentionned above, ^{40}Ti is used as a reference since its decay has already been studied extensively [15,16]. The proton energy and decay time distributions are presented in fig. 2. For energy calibration, peaks 2, 3 and 4 have been fitted. The relative intensities are reported in table 1 and are in good agreement with previous experiments. In the present experiment, the γ detection efficiency was too low to observe the 2469 keV line in ^{39}Ca in coincidence with the 1330 keV proton peak mentioned by Liu *et al.* [16] and Bhattacharya *et al.* [15].

The half-life is estimated by fitting the distribution with an exponential decay and a constant background, since there is no contribution from the decay of the daughter nucleus. The resulting value of $T_{1/2} = (53.5 \pm 2.5)$ ms is in good agreement with previous measurements and close to theoretical predictions (see table 6).

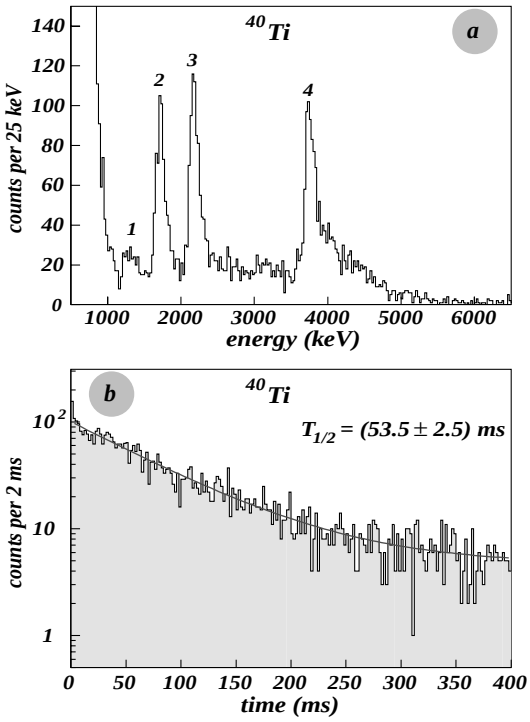

Fig. 2. a) Decay energy distribution of ^{40}Ti. The main proton lines are reported in table 1 for comparison with previous work. b) Decay time distribution of decay events after implantation of ^{40}Ti. The deduced half-life is (53.5 ± 2.5) ms (see table 6).

4.2 The decay of ^{39}Ti

The limited statistics of the present work as well as of the work from Détraz *et al.* [17] and Moltz *et al.* [18] does not allow for a detailed comparison of the energy spectra. However, from the proton spectrum in fig. 3a, it seems to be likely that the peak at (4880 ± 40) keV (marked as 4) corresponds to the β2p decay to the ground state of ^{37}K as already observed by Détraz *et al.* and Moltz *et al.* This energy is 130 keV higher than in the work of Moltz *et al.* [18] and leads to an excitation energy of the isobaric analogue state (IAS) in ^{39}Sc of (8.96 ± 0.06) MeV. From this result, we deduce a mass excess for this analog state of $\Delta m = (-5210 \pm 85)$ keV. Using the mass excess of the ^{39}Cl ground state ($\Delta m = -29799$ keV) and of the ^{39}Ar IAS ($\Delta m = -31334$ keV), the mass excess resulting from the isobaric multiplet mass equation (IMME) for ^{39}Ti is $\Delta m = 1790 \pm 90$ keV, with IMME coefficients in agreement with what is expected from a calculation with a uniformly charged sphere [24].

From this result, it follows that ^{39}Ti is unbound by 670 keV with respect to two-proton emission. This is in nice agreement with several theoretical S_{2p} values given in table 2. When we use the mass excess of the IAS in ^{39}Sc as determined in the present work to calculate the coefficients of the IMME for the $A = 39, T_z = -5/2$ nuclei, we get coefficients which are somewhat closer to the result expected from a uniformly charged sphere (the expected ratio is 1, our value is 1.1 ± 0.2) as when using the result

Table 1. Branching ratios of main proton lines in the decay of ^{40}Ti. The results of the present work are compared to data from literature.

Peak	This work		Liu *et al.* [16]		Bhattacharya *et al.* [15]	
number	E_p (keV)	b_P (%)	E_p (keV)	b_P (%)	E_p (keV)	b_P (%)
1	1332 (25)	5.8 (20)	1322 (25)	4.35 (82)	1325 (7)	3.58 (61)
2	1703 (10)	21.7 (30)	1705 (10)	22.5 (21)	1701 (6)	23.8 (6)
3	2154 (9)	27.4 (36)	2167 (10)	28.5 (19)	2160 (6)	29.8 (7)
4	3736 (14)	23.8 (36)	3731 (10)	22.8 (19)	3734 (7)	21.7 (5)

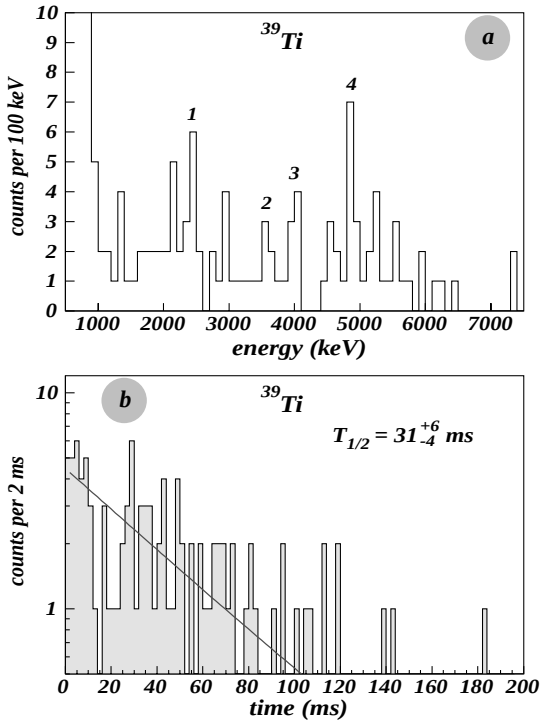

Fig. 3. a) Decay energy distribution from the decay of ^{39}Ti. The peak labels correspond to those used in table 3. b) Decay time distribution of decay events after implantation of ^{39}Ti. The fit yields a half-life of $T_{1/2} = 31^{+6}_{-4}$ ms.

Table 2. Comparison of two-proton separation energies for ^{39}Ti from the present work with theoretical predictions and with the experimental datum from Moltz *et al.*

Reference	S_{2p} (keV)
This work with IMME	-670 ± 100
Moltz *et al.* [18]	-530 ± 65
Brown [11]	-657
Cole [13]	-798 ± 39
Ormand [25]	-666 ± 107

of Moltz *et al.* (1.2 ± 0.2). However, as the error bars are large, no final conclusion is possible.

Although other proton groups are visible in the spectrum of fig. 3a, no further transition can be clearly identified to support or reject the assignment of the two-proton transition. The most prominent charged-particle groups are summarized in table 3 with their relative intensity.

Table 3. Branching ratios and decay energies of the main proton lines in the decay of ^{39}Ti. Peak 4 is suggested to correspond to the β2p decay to the ground state in ^{37}K via the IAS in ^{39}Sc.

Peak number	Energy (keV)	Branching ratio (%)
1	2440 (25)	8.0 (50)
2	3575 (30)	6.5 (45)
3	3990 (30)	7.3 (45)
4	4880 (40)	12.5 (65)

As ^{39}Sc is unbound, the decay of ^{39}Ti proceeds with a 100% branching ratio via delayed-particle emission. From fig. 3b, we deduce a half-life of $T_{1/2} = 31^{+6}_{-4}$ ms for ^{39}Ti which is in good agreement with predicted values and previous experimental work [17] (see table 6). There is no contamination in the proton energy distribution from the decay of ^{38}Ca (βp daughter) or ^{37}K (β2p daughter) which are much longer lived and do not decay via proton emission.

4.3 The decay of ^{43}Cr

The proton energy distribution of the decay of ^{43}Cr is shown in fig. 4a. Using the mass evaluation of Audi and Wapstra [26], we assign the charged-particle peak labelled 9 to the β2p decay via the IAS in ^{43}V to the ground state in ^{41}Sc. This interpretation is supported by the fact that this peak has a somewhat larger width than those for other transitions which might be explained by the different relative angles between the two protons yielding different recoil energies for the heavy fragment. As the energy loss of the heavy recoil is subject to a strong pulse height defect [27], two-proton lines are usually broadened. From this information, the excitation energy of the IAS in ^{43}V is deduced to be $(8250 \pm 25 \pm 230)$ keV, where the second uncertainty comes from the ^{43}V mass extrapolation.

The γ-energy distribution (see fig. 5) in coincidence with protons shows a strong γ line at (1553.5 ± 1.0) keV. As shown in fig. 5a, this γ peak shows up in coincidence with all charged-particle peaks all over the decay energy distribution. As this γ-ray de-excites the first excited state in ^{42}Ti, we conclude on only a very small proton branching to the ground state of ^{42}Ti.

Another line at (1938 ± 2) keV is seen in coincidence with the charged-particle peak 10 at $E = 4590$ keV (see fig. 5b). Such a γ transition is neither known in ^{42}Ti (βp daughter) nor in ^{41}Sc (β2p daughter). If we assume that the β feeding above the IAS in ^{43}V is weak, the 4590 keV

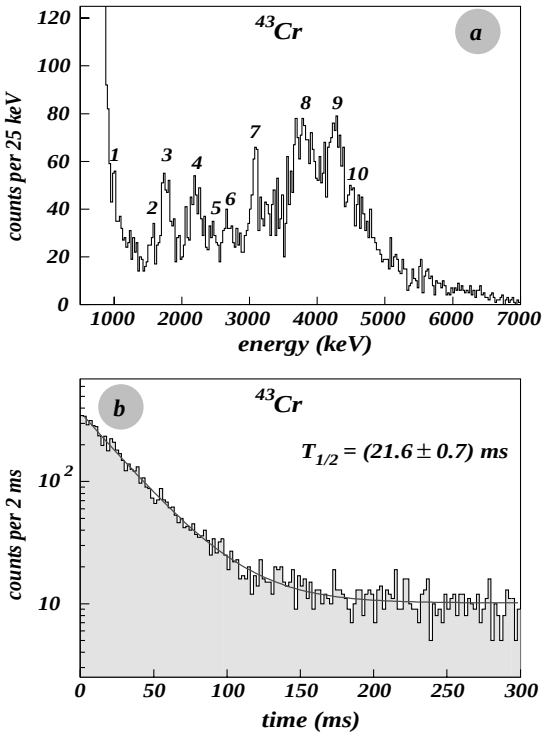

Fig. 4. a) Decay energy distribution in the decay of ^{43}Cr. The peak labels correspond to those in table 4. Peak 9 is tentatively identified as originating from a β2p transition via the IAS in ^{43}V. b) Decay time distribution of decay events after implantation of ^{43}Cr. A half-life of (21.6±0.7) ms is deduced.

Table 4. Branching ratios and decay energies of the main charged-particle groups in the decay of ^{43}Cr. The labels correspond to those used in fig. 4a.

Peak number	Energy (keV)	Branching ratio (%)
1	1008 (17)	2.0 (6)
2	1563 (18)	2.3 (7)
3	1780 (16)	6.0 (12)
4	2222 (16)	6.4 (13)
5	2500 (21)	3.3 (9)
6	2717 (22)	4.0 (10)
7	3078 (16)	7.7 (12)
8	3828 (23)	18.3 (21)
9	4292 (22)	14.8 (2.8)
10	4590 (45)	3.8 (20)

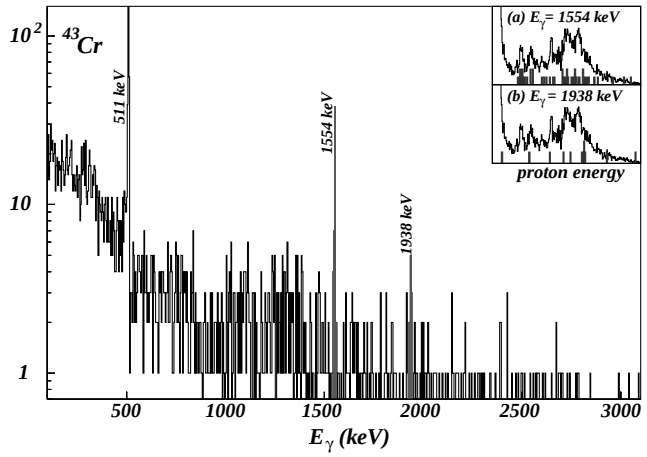

Fig. 5. γ-energy spectrum as measured in coincidence with charged particles. The insert a) shows the charged-particle events in coincidence with the 1554 keV γ line. It evidences that this γ line is in coincidence with almost all charged-particle groups. The 1938 keV line is mainly in coincidence with proton peak 10 (insert b).

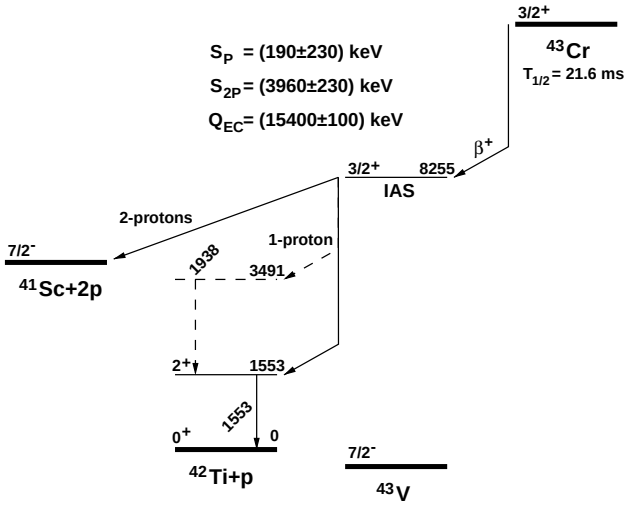

Fig. 6. Partial decay scheme for ^{43}Cr as deduced from the present work.

peak cannot originate from a β2p decay, as the Q value for a transition from the IAS to the ^{41}Sc ground state is only about 4 MeV. A consistent picture arises if we assume that the 4590 keV line links the IAS to an excited state in ^{42}Ti at 3492 keV. This state would decay by a γ cascade of the 1938 keV and the 1554 keV γ-rays. Such a level is not known in ^{42}Ti, but this might be explained by the fact that this nucleus is only poorly studied. In the mirror nucleus ^{42}Ca, a $I^\pi = 3^-$ level is known at 3446.96 MeV which indeed decays by a cascade of γ-rays of 1922.18 keV and 1524.73 keV. However, if the assumed spins (see fig. 6) are correct, such a transition would be a $\ell = 1$ transition and should be suppressed. Nevertheless, such a hypothesis leads to an excitation energy of the IAS in ^{43}V of $(8270 \pm 45 \pm 230)$ keV ($\pm$230 keV from the ^{43}V mass uncertainty) in good agreement with the one deduced from the β2p transition as mentioned above. The energy resulting from both estimates is then $E^*_{\rm IAS} = (8255 \pm 25 \pm 230)$ keV. With this information, we propose the partial decay scheme shown in fig. 6.

The half-life of ^{43}Cr was determined in the usual way with a condition on the charged-particle spectrum to select events with a decay energy above 1 MeV. We deduce a half-life of $T_{1/2} = (21.6 \pm 0.7)$ ms (see fig. 4b). This value is in agreement with but much more precise than the value from Borrel *et al.* [19] of 27^{+32}_{-10} ms.

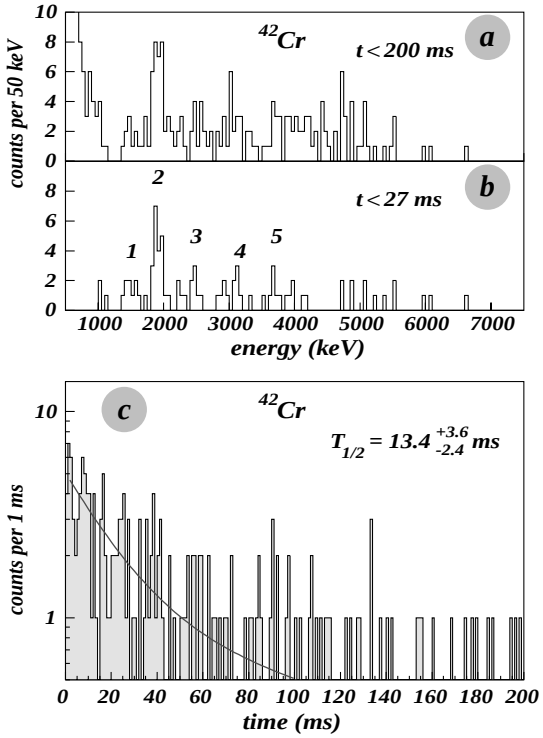

Fig. 7. a,b) Decay energy distribution in the decay of ^{42}Cr. The histogram in part a) shows the decay energy for events decaying up to 200 ms after a ^{42}Cr implantation, whereas the histogram in b) is due to events up to 27 ms corresponding to two half-lives. The short-time cut favors mainly events from the short-lived ^{42}Cr (see table 5), while the daughter decay contribute to the 200 ms histogram. c) Time distribution of decay events after implantation of ^{42}Cr. The fit includes the contribution of the decay of ^{41}Ti.

Table 5. Branching ratios and decay energies of the main charged-particle groups in the decay of ^{42}Cr. The peak numbers correspond to those used in fig. 7b.

Peak number	Energy (keV)	Branching ratio (%)
1	1500 (35)	9.2 (73)
2	1905 (20)	29.2 (100)
3	2490 (30)	9.2 (73)
4	3110 (20)	7.7 (42)
5	3715 (20)	6.2 (40)

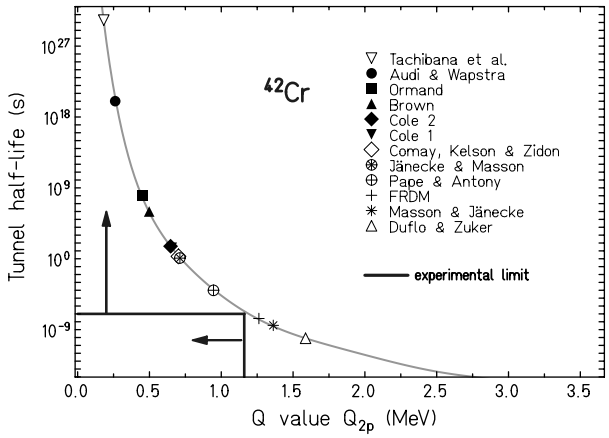

Fig. 8. Barrier penetration half-life of ^{42}Cr for the tunneling of a di-proton through the Coulomb barrier as a function of the two-proton separation energy. Q_{2p} values resulting from different mass models [28,26,11–13,29–31] are shown.

4.4 The decay of ^{42}Cr

The isotope ^{42}Cr is a possible candidate for two-proton radioactivity. However, according to all theoretical predictions [11–13], its Q_{2p} value is probably too small for a detectable two-proton branching ratio. Our experimental results are in agreement with this expectation. When inspecting the charged-particle spectrum in fig. 7a,b, the most prominent peak is the line at 1.9 MeV. If this peak were due to two-proton radioactivity, the barrier penetration half-life of ^{42}Cr would be of the order of 10^{-12} s, orders of magnitude lower than the flight time from the production target to the detector, and this isotope would decay on its flight through the separator (see fig. 8). The observation of ^{42}Cr in our experiment and in previous work rejects several models predicting ^{42}Cr highly unbound with Q_{2p} values of 1 MeV and higher.

Another hint against a two-proton decay of ^{42}Cr is the half-life determined for charged-particle events with an energy above 1 MeV (fig. 7c). Our experimental data yield a half-life of $T_{1/2} = 13.4^{+3.6}_{-2.4}$ ms. Such a half-life is typical for a β decay in this region. We therefore conclude that ^{42}Cr is decaying mainly by β-delayed charged-particle emission and that a possible two-proton radioactivity is very weak.

Each β decay of ^{42}Cr is followed by a proton emission since the daughter nucleus, ^{42}V, is unbound. In the case of a βp transition, the decay is followed by another βp emission from ^{41}Ti with a half-life of (82 ± 3) ms [16]. In the proton spectrum of fig. 7a,b, two cuts at $t = 200$ ms and $t = 27$ ms (corresponding to two half-lives) have been performed in order to discriminate contributions from ^{41}Ti and ^{42}Cr. From this analysis, we conclude that the charged-particle group at 1.9 MeV is due to the decay of ^{42}Cr. However, due to too low statistics and therefore no coincident γ-rays, we cannot attribute this peak to a well-defined transition.

Besides the peak at 1.9 MeV, no other pronounced structure appears in the spectrum. The transition strength located around 4 to 5 MeV is probably due to the daughter decay of ^{41}Ti [16]. According to the structure of the mirror nucleus of ^{40}Sc, the 2490 keV charged-particle line could be the $\ell = 0$ two-proton transition from the IAS to the first excited 0^+ state in ^{40}Sc which, according to its mirror ^{40}K lies at around 1.6 MeV, but the statistics is too low to observe a coincident γ-ray.

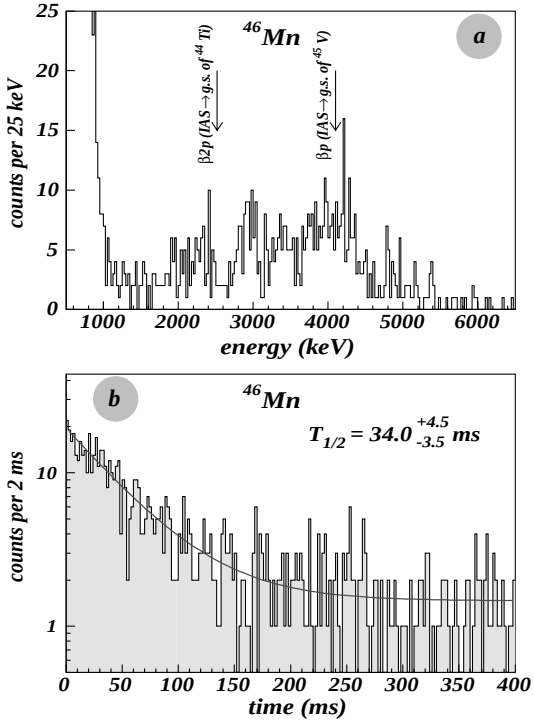

Fig. 9. a) Decay energy distribution of ^{46}Mn. The arrows indicate the expected positions of charged-particle groups from βp and β2p transitions via the IAS to the ground states of ^{45}V and ^{44}Ti. b) Decay time distribution of events after implantation of ^{46}Mn. The half-life deduced is $T_{1/2} = 34.0^{+4.5}_{-3.5}$ ms.

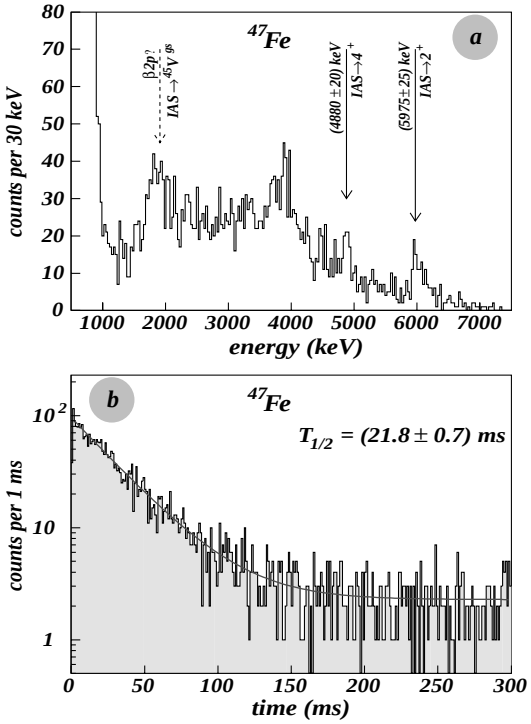

Fig. 10. a) Decay energy spectrum of ^{47}Fe. The arrows indicate the charged-particle groups from the decay of the IAS to the first and second excited state in ^{46}Cr. *b*) Decay time distribution of decay events after implantation of ^{47}Fe. The half-life deduced is $T_{1/2} = (21.8 \pm 0.7)$ ms.

4.5 The decay of ^{46}Mn

Figure 9a shows the decay energy distribution of ^{46}Mn. The expected positions for βp and β2p transitions via the IAS in ^{46}Cr to the ground states of ^{45}V and ^{44}Ti are indicated as determined from the mass evaluation of Audi and Wapstra [26], but no peak can be clearly identified. The spectrum rather resembles the typical bell-shaped proton distribution which is obtained when a high number of states is populated which then decay by proton emission (see, *e.g.*, [32]). Much higher statistics is needed to locate decay energy peaks linked for example to the decay of the IAS.

For this isotope, the half-life is determined to be $T_{1/2} = 34.0^{+4.5}_{-3.5}$ ms. No subsequent decay by proton emission is expected to contaminate the decay energy distribution above 1 MeV. This result is in agreement with a previous result from Borrel *et al.* [19] (see table 6). From the trigger efficiency and the number of counts in the decay energy distribution, we deduce a total proton branching ratio of $P_{\rm p} = (58 \pm 9)\%$.

4.6 The decay of ^{47}Fe

In fig. 10a, we present our results for the charged-particle emission from ^{47}Fe. We will analyse this spectrum together with the coincident γ-ray spectrum shown in fig. 11.

According to the structure of the mirror nucleus of the β-decay daughter ^{47}Mn, we suppose that the transition at $E_{\rm p} = (5975 \pm 25)$ keV (see fig. 10a) corresponds to the delayed proton emission from the IAS in ^{47}Mn to the first 2^+ state in ^{46}Cr. This assumption is supported by the coincident observation of a γ line at (892 ± 1) keV (see fig. 11a) which most probably corresponds to the $2^+ \rightarrow 0^+$ transition in ^{46}Cr. In the mirror nucleus ^{46}Ti, the 2^+ state has an excitation energy of 889.3 keV. Using the ground-state mass excess of ^{46}Cr, we deduce an excitation energy of the IAS of $E^* = (6867 \pm 30 \pm 160)$ keV, where the second error bar is due the ^{47}Mn mass excess uncertainty.

In agreement with this excitation energy, we can assign the (4880±20) keV charged-particle peak to the transition from the IAS to the first 4^+ state in ^{46}Cr. In the γ-ray spectrum (see fig. 11b), the 1095 keV line (1120.5 keV in the mirror nucleus), in coincidence with the 4880 keV peak, corresponds then to the $4^+ \rightarrow 2^+$ transition. This assignment leads to an excitation energy of the IAS of $E^* = (6869 \pm 25 \pm 160)$ keV which is in nice agreement with the result above. We deduce a mean value for the position of this IAS of $E^* = (6868 \pm 35 \pm 160)$ keV. The observation of the two γ-rays belonging to the ground-state rotational band of the even-even nucleus ^{46}Cr is in agreement with what is expected from mirror symmetry.

According to the structure of the mirror nucleus of ^{46}Cr, the strong proton transition around (3890 ± 25) keV may correspond to the decay of the IAS to states around

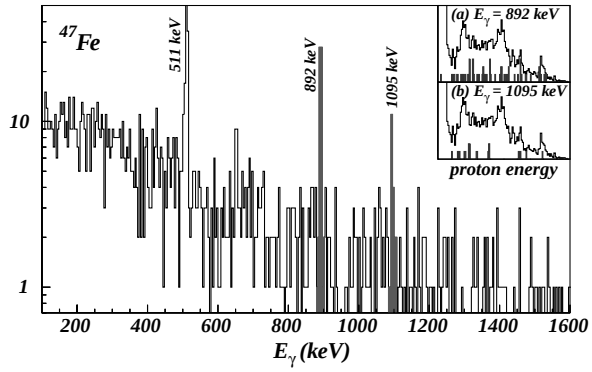

Fig. 11. γ-ray energies measured in coincidence with protons. Inserts a) and b) show the distribution of charged-particle events in coincidence with the 892 and 1095 keV γ lines in comparison to the complete decay energy distribution.

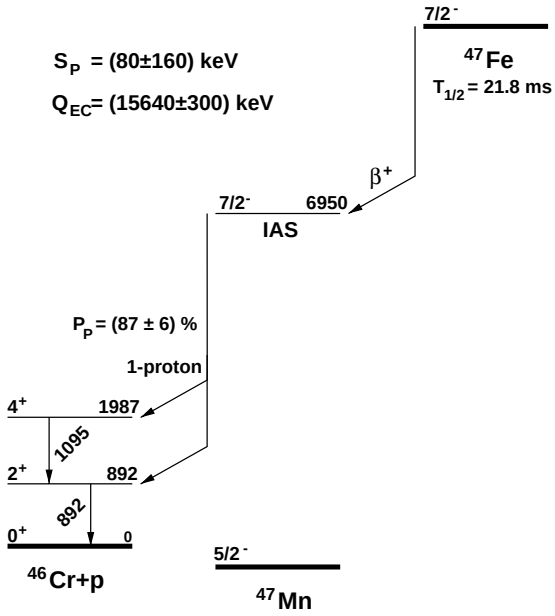

Fig. 12. Partial decay scheme for ^{47}Fe. Energies on the scheme are given in keV.

3 MeV excitation energy, where states with spin $J^\pi = 2^+, 3^-, 4^-$ are expected which could be fed by proton emission with low angular momentum ($\ell = 0, 1$) from the IAS. However, this strength can also result from proton emission by low-lying states in ^{47}Mn populated by Gamow-Teller decays of ^{47}Fe.

The β2p transition via the IAS ($J^\pi = 7/2^-$) to the ground state of ^{45}V is expected around 1915 keV. Some proton strength is observed at this energy, but no single peak can be clearly resolved. According to calculation by Detraz [17] the ratio between β2p and βp emission from the IAS is rather low (less than 0.05). This prediction is in agreement with the absence of a strong β2p peak in our experimental spectrum.

All protons in the charged-particle spectrum of fig. 10a are due to the decay of ^{47}Fe. We deduce the half-life in the usual way and obtained a value of $T_{1/2} = (21.8 \pm 0.7)$ ms,

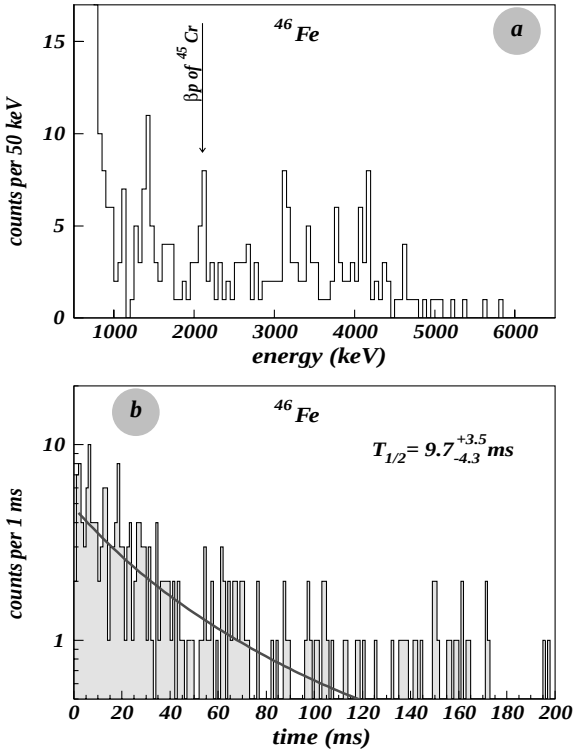

Fig. 13. a) Decay energy distribution of ^{46}Fe. The peak from the daughter decay of ^{45}Cr at 2.1 MeV is indicated. b) Decay time distribution of events after implantation of ^{46}Fe. The resulting half-life is $T_{1/2} = 9.7^{+3.5}_{-4.3}$ ms.

which is in agreement with but more precise than a previous measurement [19]. As a final result, we determine the proton branching ratio to be $P_\mathrm{p} = (87 \pm 7)\%$ for protons above 1 MeV. The resulting decay scheme is shown in fig. 12.

4.7 The decay of ^{46}Fe

For the $A = 46$, $T = 3$ nuclei, three members of the isobaric mass multiplet are probably known. We will use therefore the ground state of ^{46}Ca, the 5.021 MeV state in ^{46}Sc, and the 14.153 MeV state in ^{46}Ti. For the IMME, we obtain the following mass excess values: (-43.135 ± 3) MeV (^{46}Ca), (-36.738 ± 0.006) MeV (^{46}Sc), and (-29.972 ± 0.007) MeV (^{46}Ti). With these data, we get the mass excess values for ^{46}Fe and for the IAS in ^{46}Mn of (0.769 ± 0.115) MeV and (-7.468 ± 0.072) MeV, respectively. There is a slight uncertainty concerning the state in ^{46}Ti, because there is a neighboring state at 14.300 MeV state with a tentative assignment of $I^\pi = 0^+$. However, whereas the 14.153 MeV state yields parameters close to those expected from a uniformly charged sphere [24] and a ^{46}Fe ground-state mass close to the mass evaluation of Audi and Wapstra [26], the 14.300 MeV state gives values far away from both criteria. Using these mass excess values, we expect the βp transition via the IAS to the ground state of ^{45}Cr at about 4.65 MeV in the decay energy spec-

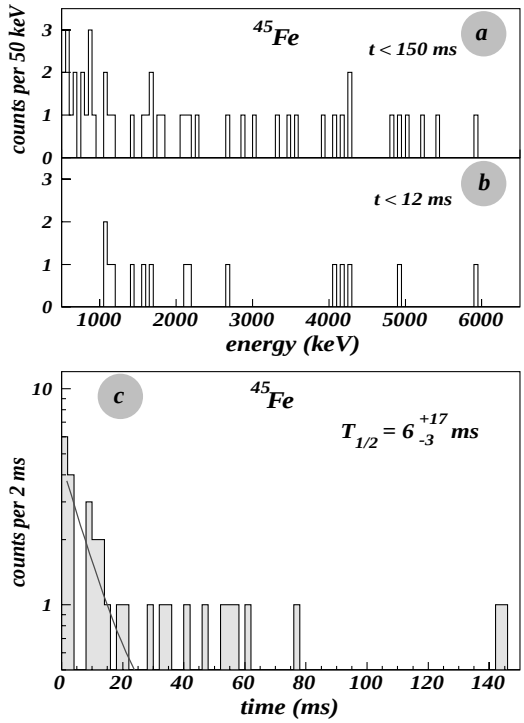

Fig. 14. a, b) Decay energy spectra of ^{45}Fe. The histogram in part a) is due to events up to 150 ms after a ^{45}Fe implantation, whereas the spectrum in b) contains decay events occurring less than 12 ms after the implantation. c) Decay time distribution of events after implantation of ^{45}Fe yielding a half-life of $T_{1/2} = 6^{+17}_{-3}$ ms.

trum. The β2p transition to the ground state of ^{44}V is expected at 1.8 MeV.

Figure 13a shows the charged-particle spectrum from the decay of ^{46}Fe. No peak is seen for the β2p transition to the ground state. This is in agreement with the calculations of Detraz [17] who predicts a ratio between β2p and βp of less than 10%.

Although we have clearly seen several charged-particle lines in the decay energy spectrum of fig. 13a, we cannot place any of them in a decay scheme. Proton-γ coincidences are necessary to identify the transitions involved.

The βp decay of ^{46}Fe feeds states in ^{45}Cr. The decay of this isotope has been studied by Jackson *et al.* [33] who identified a delayed proton branch with an energy of 2.1 MeV. This peak is visible in our spectrum. From the intensity of this peak and the known branching ratio for this 2.1 MeV proton group, we deduce a βp branching ratio of (36 ± 20) % for ^{46}Fe. As the expected β2p branching ratio is much smaller [17], more than 50% of the decay of ^{46}Fe feeds proton-bound levels in ^{46}Mn. For a rather exotic isotope like ^{46}Fe with a β-decay daughter having a one-proton separation energy of only about 300 keV, a 50% feeding of γ-decaying levels or of the ground state of ^{46}Mn seems to be rather high. From the mirror nucleus, only one $I^\pi = 1^+$ level is expected in ^{46}Mn at around 1 MeV which might not decay by proton emission. Using the mass excess of ^{46}Fe as determined in the preceeding paragraph, the mass excess of ^{46}Mn [26], and the half-life of ^{46}Fe (see below), a 50% branching ratio to a state at about 1 MeV corresponds to a log ft value of 3.2, much too small for a Gamow-Teller transition. A possible explanation for this discrepancy might be a much larger β2p strength. However, higher-statistics data are clearly needed to get a consistent picture for the decay of ^{46}Fe.

Taking into account the daughter decay branches in ^{45}Cr and ^{46}Mn, the resulting half-life for ^{46}Fe is $T_{1/2} = 12.0^{+4.2}_{-3.2}$ ms (fig. 13b) where the uncertainty is the quadratic sum of uncertainties coming from the fit, the daughter half-lives and the branching ratios.

4.8 The decay of ^{45}Fe

According to theoretical predictions [11–13], ^{45}Fe together with ^{48}Ni is the best candidate for two-proton radioactivity, *i.e.* a correlated emission of two protons from the ground state. In such a case, due to their low energy, the protons may not exit the implantation detector and we would measure only the sum energy of the decay. However, since the acquisition was triggered only by events in the neighbouring detector, these 2p events are lost and we should, in the case of a 2p radioactivity, only observe the βp decay of the daughter nucleus ^{43}Cr.

In the decay energy spectra of fig. 14a,b, we distinguish again fast decays which occur within 12 ms after a ^{45}Fe implantation and events occuring in a time interval up to 150 ms which should favour the observation of the daughter and grand-daughter decay. However, the very poor statistics prevents any conclusion based on this spectrum. Charged-particle groups would be expected at about 11.3, 8.5 and 8.3 MeV in the case of βp, β2p, or β3p transition via the IAS to the respective ground states. No counts are observed in these regions due to the fact that i) the proton emission might involve excited states in the grand-daughter nuclei and ii) the proton peak efficiency decreases drastically for these high proton energies.

The most valuable information is probably contained in the decay time distribution shown in fig. 14c. The value is determined from a fit taking into account different possibilities for the daughter decay. The only contamination of the half-life determination comes from the daughter decay of ^{44}Cr. However, as the decay characteristics of this nucleus are unknown, we assume that it might decay with a branching ratio between 0 and 20% by delayed-proton emission. This hypothesis is based on the decay properties of ^{52}Ni [34] and ^{48}Fe [35]. Our fitting procedure yields a half-life of $T_{1/2} = 6^{+17}_{-3}$ms (fig. 14c). This rather rough estimate of the half-life may be compared to theoretical β-decay half-lives as shown in table 6. The theoretical values are compatible with our experimental datum and indicate therefore that ^{45}Fe might decay mainly by β decay and not by two-proton radioactivity. However, higher-statistics data are clearly needed before concluding on the main decay mode of this isotope.

Table 6. Comparison of theoretical predictions for β-decay half-lives to results from previous experiments and from the present work. All values are given in ms.

Isotope	Theoretical prediction			Experimental half-life	
	Gross theory [31]	Ormand [12]	Hirsch *et al.* [37]	Previous work	This work
^{40}Ti	56	56	–	54 ± 2 [(a)]	53.5 ± 2.5
				52.7 ± 1.5 [(b)]	
^{39}Ti	28	29	–	26^{+8}_{-7} [(c)]	31^{+6}_{-4}
^{43}Cr	21	14	23 - 57	21 ± 4 [(d)]	21.6 ± 0.7
^{42}Cr	21.2	17	12 - 33	–	$13.4^{+3.6}_{-2.4}$
^{46}Mn	35	37	–	41^{+7}_{-6} [(d)]	$34.0^{+4.5}_{-3.5}$
^{47}Fe	27.3	–	22 - 57	27^{+32}_{-10} [(d)]	21.8 ± 0.7
^{46}Fe	24.3	18	15 - 30	20^{+20}_{-8} [(d)]	$9.7^{+3.5}_{-4.3}$
^{45}Fe	11.7	7	7 - 30	–	6.0^{+17}_{-3}
^{49}Ni	10.7	–	7 - 20	–	12^{+5}_{-3}

[(a)] From W. Liu *et al.* [16].
[(b)] From W. Bhattacharya *et al.* [15].
[(c)] From C. Detraz *et al.* [17].
[(d)] From V. Borrel *et al.* [19].

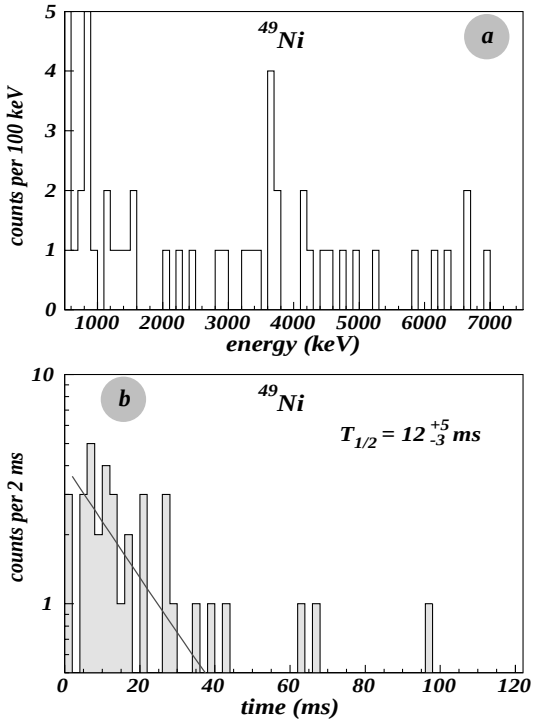

Fig. 15. a) Decay energy spectrum of ^{49}Ni. The peak at 3.7 MeV is identified as being due to delayed charged-particle emission (see text). b) Decay time distribution of events after implantation of ^{49}Ni yielding a half-life of $T_{1/2} = 12^{+5}_{-3}$ ms.

4.9 The decay of ^{49}Ni

Like ^{42}Cr, ^{49}Ni is a possible candidate for 2p radioactivity. However, similar to ^{42}Cr, theoretical calculations predict that this isotope should decay mainly or even exclusively by β-delayed charged-particle channels.

Figures 15a and b present the decay energy and decay time distribution for ^{49}Ni. Although β-delayed charged-particle emission from the IAS in ^{49}Co is energetically allowed ($Q_{\rm p} \sim 10.5$, $Q_{\rm 2p} \sim 7.3$, and $Q_{\rm 3p} \sim 7.2$ MeV [26]), only one transition is clearly identified in the energy spectrum. The six events at around 3.7 MeV are clearly not due to 2p radioactivity, because in such a case the barrier penetration half-life would be as short as 10^{-16} s, many orders of magnitude smaller than the flight time through the LISE3 separator. This peak is rather due to a β-delayed charged-particle branch. However, due to the poor statistics for this nucleus, no coincident γ-rays were observed. Therefore, we can not attribute the 3.7 MeV line to any well-defined transition.

To estimate the half-life of ^{49}Ni, our experimental results do not allow to discriminate the different possible decay channels. Détraz [36] calculated a β2p/βp ratio of 3 for this nucleus. If the decay proceeds by delayed one-proton emission to ^{48}Fe, we expected a subsequent βp emission in less than 20% of the decays [34]. The β2p or β3p channels are only followed by very weak delayed-particle emission channels. Therefore, taking into account a possible contamination from the βp decay of ^{48}Fe in 0 to 10% of the decays of ^{49}Ni, we obtain a half-life of $T_{1/2} = 12^{+5}_{-3}$ ms. This value is in reasonable agreement with β-decay half-life calculations (see table 6). From this comparison we conclude, as from the decay energy spectrum, that ^{49}Ni most probably decays by β emission.

5 Concluding remarks

The present experiment performed at the GANIL/LISE3 facility using the fragmentation of a ^{58}Ni primary beam yielded valuable spectroscopic information concerning the decay of nuclei in the region from titanium to nickel very close to or even beyond the proton drip-line. First half-life

values have been determined for ^{42}Cr, ^{45}Fe and ^{49}Ni. In addition, higher-precision values have been obtained for ^{39}Ti, ^{43}Cr, ^{46}Mn and ^{46,47}Fe.

Although only few transitions could be clearly identified, delayed-proton or two-proton emission was used to determine the excitation energy of the IAS in the decay of ^{43}Cr and ^{47}Fe. However, the precision obtained is strongly limited by the lack of precise ground-state mass excess values of isotopes involved in the decays. Despite the low detection efficiency, proton-γ coincidences proved to be a helpful tool to identify transitions in the decays of ^{43}Cr and ^{47}Fe and they give valuable information on the decay scheme and the daughter-nucleus structure.

One of the purposes of decay studies in this mass region is to search for two-proton radioactivity, since ^{39}Ti, ^{42}Cr, ^{45}Fe and ^{48,49}Ni are candidates to this decay process. We did not observe this process. However, an improved detection set-up optimised for such a search, together with increased statistics should allow to search for such a decay mode especially in the decay of ^{45}Fe, ^{48}Ni, and ^{54}Zn.

We would like to acknowledge the continous effort of the GANIL accelerator staff to provide us with a stable, high-intensity beam. We express our sincere gratitude to the LISE staff for ensuring a smooth running of the LISE3 separator. This work was supported in part by the Polish Committee of Scientific Research under grant KBN 2 P03B 036 15, the contract between IN2P3 and Poland, as well as by the Conseil Régional d'Aquitaine.

References

1. B. Blank, S. Andriamonje, S. Czajkowski, F. Davi, R. Del Moral, J.P. Dufour, A. Fleury, A. Musquère, M.S. Pravikoff, R. Grzywacz, Z. Janas, M. Pfützner, A. Grewe, A. Heinz, A. Junghans, M. Lewitowicz, J.-E. Sauvestre, C. Donzaud, Phys. Rev. Lett. **74**, 4611 (1995).
2. B. Blank, M. Chartier, S. Czajkowski, J. Giovinazzo, M.S. Pravikoff, J.-C. Thomas, G. de France, F. de Oliveira Santos, M. Lewitowicz, C. Borcea, R. Grzywacz, Z. Janas, M. Pfützner, Phys. Rev. Lett. **84**, 1116, (2000)
3. M.D. Cable, J. Honkanen, R.F. Parry, S.H. Zhou, Z.Y. Zhou, J. Cerny, Phys. Rev. Lett. **50**, 404 (1983).
4. M.D. Cable, J. Honkanen, E. Schloemer, M. Ahmed, J.E. Reiff, Z.Y. Zhou, and J. Cerny, Phys. Rev. C **30**, 1276 (1984).
5. R. Jahn, R.L. McGrath, D.M. Moltz, J. Reiff, X.J. Xu, J. Äystö, and J. Cerny, Phys. Rev. C **31**, 1576 (1985).
6. L. Axelsson, J. Äystö, M. Borge, L. Fraile, H. Fynbo, A. Honkanen, P. Hornshoj, A. Jokinen, B. Jonson, P. Lipas, I. Martel, J. Mukha, T. Nilsson, G. Nyman, B. Petersen, K. Rissager, M. Smedberg, O. Tengblad, Nucl. Phys. A **628**, 345 (1998).
7. V. Borrel, J. Jacmart, F. Pougheon, A. Richard, R. Anne, D. Bazin, H. Delagrange, C. Détraz, D. Guillemaud-Mueller, A. Mueller, E. Roeckl, M. Saint-Laurent, J. Dufour, F. Hubert, M. Pravikoff, Nucl. Phys. A **473**, 331 (1987).
8. J. Äystö, D.M. Moltz, X. Xu, J. Reiff, J. Cerny, Phys. Rev. Lett. **55**, 1384 (1985).
9. R.A. Kryger, A. Azhari, M. Hellström, J.H. Kelley, T. Kubo, R. Pfaff, E. Ramakrishnan, B.M. Sherrill, M. Thoennessen, S. Yokoyama, R.J. Charity, J. Dempsey, A. Kirov, N. Robertson, D.G. Sarantites, L.G. Sobotka, and J.A. Winger, Phys. Rev. Lett. **74**, 860 (1995).
10. O.V. Bochkarev, A.A. Korsheninnikov, E.A. Kuz'min, I.G. Mukha, L.V. Chulkov, G.B. Yan'kov, Sov. J. Nucl. Phys. **55**, 955 (1992).
11. B.A. Brown, Phys. Rev. C **43**, R1513 (1991).
12. W.E. Ormand, Phys. Rev. C **55**, 2407 (1997).
13. B.J. Cole, Phys. Rev. C **54**, 1240 (1996).
14. E. Caurier, A.P. Zuker, A. Poves, G. Martinez-Pinedo, Phys. Rev. C **50**, 225 (1994).
15. A.G.M. Bhattacharya, N.I. Kaloskamis, E.G. Adelberger, H.E. Swanson, R. Anne, M. Lewitowicz, M.G. Saint-Laurent, W. Trinder, C. Donzaud, D. Guillemaud-Mueller, S. Leenhardt, A.C. Mueller, F. Pougheon, and O. Sorlin, Phys. Rev. C **58**, 3677 (1998).
16. W. Liu, M. Hellstrom, R. Collatz, J. Benlliure, L. Chulkov, D. Cortina Gil, F. Farget, H. Grawe, Z. Hu, N. Iwasa, M. Pfützner, A. Piechaczek, R. Raabe, I. Reusen, E. Roeckl, G. Vancraeynest, A. Wöhr, Phys. Rev. C **58**, 2677 (1998).
17. C. Détraz, R. Anne, P. Bricault, D. Guillemaud-Mueller, M. Lewitowicz, A.C. Mueller, Y.H. Zhang, V. Borrel, J.C. Jacmart, F. Pougheon, A. Richard, D. Bazin, J.P. Dufour, A. Fleury, F. Hubert, M.S. Pravikoff, Nucl. Phys. A **519**, 529 (1990).
18. D.M. Moltz, J.C. Batchelder, T.F. Lang, T.J. Ognibene, J. Cerny, P.E. Haustein, P.L. Reeder, Z. Phys. A **342**, 273 (1992).
19. V. Borrel, R. Anne, D. Bazin, C. Borcea, G.G. Chubarian, R. Del Moral, C. Détraz, S. Dogny, J.P. Dufour, L. Faux, A. Fleury, L.K. Fifield, D. Guillemaud-Mueller, F. Hubert, E. Kashy, M. Lewitowicz, C. Marchand, A.C. Mueller, F. Pougheon, M.S. Pravikoff, M.G. Saint-Laurent, O. Sorlin, Z. Phys. A **344**, 135 (1992).
20. A. Joubert et al., *Proceedings of the Second Conference of the IEEE Particle Accelerator, San Francisco, May 1991*, edited by L. Lizama and J. Chew (IEEE, Piscataway, NJ, 1991) p. 594.
21. A.C. Mueller, R. Anne, Nucl. Instrum. Methods B **56**, 559 (1991).
22. O. Tarasov et al., *Proceedings of the 5th Conference on Radioactive Nuclear Beams, Divonne, France*, to be published (http://dnr080.jinr.ru/lise.html).
23. CN/ASD Group, PAW Users Guide, CERN Program Library Q121, CERN (1993).
24. W. Benenson, E. Kashy, Rev. Mod. Phys. **51**, 527 (1979).
25. W.E. Ormand, Phys. Rev. C **53**, 214 (1996).
26. G. Audi, A.H. Wapstra, Nucl. Phys. A **625**, 1 (1997).
27. A. Ratkowski, Nucl. Instrum. Methods **130**, 533 (1975).
28. P. Haustein, At. Data Nucl. Data Tables **39**, 185 (1988).
29. P. Möller, J.R. Nix, W.D. Myers, W.J. Swiatecki, At. Data Nucl. Data Tables **59**, 185 (1995).
30. J. Duflo, A. Zuker, Phys. Rev. C **52**, R23 (1995).
31. T. Tachibana, M. Yamada, Y. Yoshida, Prog. Theor. Phys. **84**, 641 (1990).
32. J. Giovinazzo, P. Dessagne, C. Miehé, Nucl. Phys. A **674**, 394, (2000).
33. K.P. Jackson, J.C. Hardy, H. Schmeing, R.L. Graham, J.S. Geiger, K.W. Allen, Phys. Lett. B **49**, 341 (1974).

34. L. Faux, S. Andriamonje, B. Blank, R. Del Moral, J.P. Dufour, A. Fleury, T. Josso, M.S. Pravikoff, S. Czajkowski, Z. Janas, A. Piechaczek, E. Roeckl, K.-H. Schmidt, K. Sümmerer, W. Trinder, M. Weber, T. Brohm, H.-G. Clerc, A. Grewe, E. Hanelt, A. Heinz, A. Junghans, C. Röhl, S. Steinhäuser, B. Voss, M. Pfützner, Nucl. Phys. A **602**, 167 (1996).
35. L. Faux, M.S. Pravikoff, S. Andriamonje, B. Blank, R. Del Moral, J.-P. Dufour, A. Fleury, C. Marchand, K.-H. Schmidt, K. Sümmerer, T. Brohm, H.-G. Clerc, A. Grewe, E. Hanelt, B. Voss, C. Ziegler, Phys. Rev. C **49**, 2440 (1994).
36. C. Détraz, Z. Phys. A **340**, 227 (1991).
37. M. Hirsch, A. Staudt, K. Muto, H.V. Klapdor-Kleingrothaus, At. Data Nucl. Data Tables **53**, 165 (1993).